Supplemental Figures

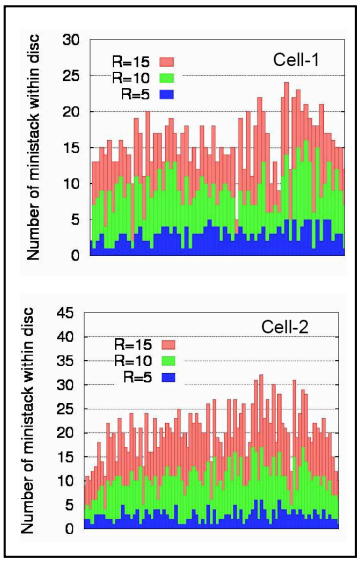

Figure S1. Random distribution of ministacks in nocodazole-treated cells as confirmed by the following test: in pre-assembly snapshots of scattered Golgi-ministacks, a circular disc of radius 5μm (25 pixel) is placed randomly in the cell and the number of mini-stacks within the disc is counted (blue). The bar graph shows almost a constant number of mini-stacks found within the disc as it is moved randomly throughout the cell. Larger discs of radius 10 μm (green) or 15 μm (red) show similar behavior. The average number of mini-stacks within the disc increases proportionally to the area of the disc. Two examples are shown.

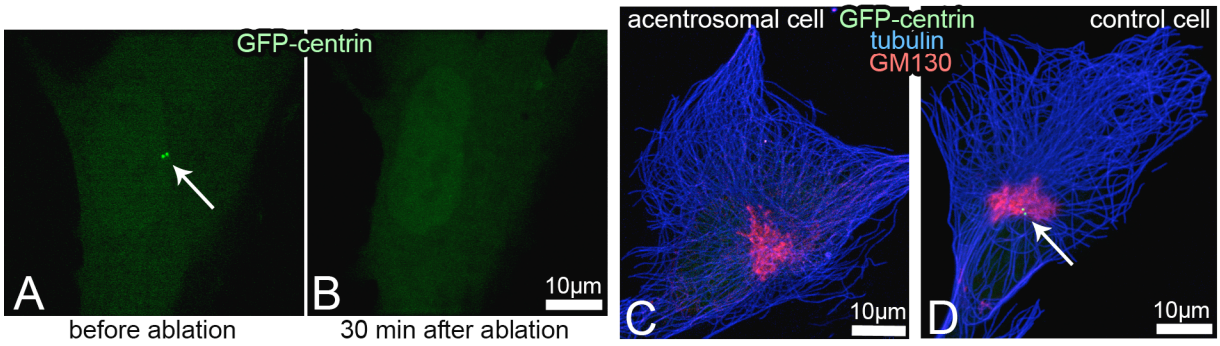

Figure S2. Centrosome ablation does not disrupt the Golgi or the MT network. A-B, an RPE1 cell expressing centrin-GFP before and after laser ablation of the centrosome (arrows). This cell was fixed after 2 hours of random migration and immunostained for the Golgi marker GM130 and MTs. **C**, Immunofluorescence image of the cell presented in A-B. GM130, red. Tubulin (far-red, false-colored blue). **D**, A bystander cell in the same preparation. Notice the intact centrosome (arrow). Golgi morphology and the MT network look similar in C and D.

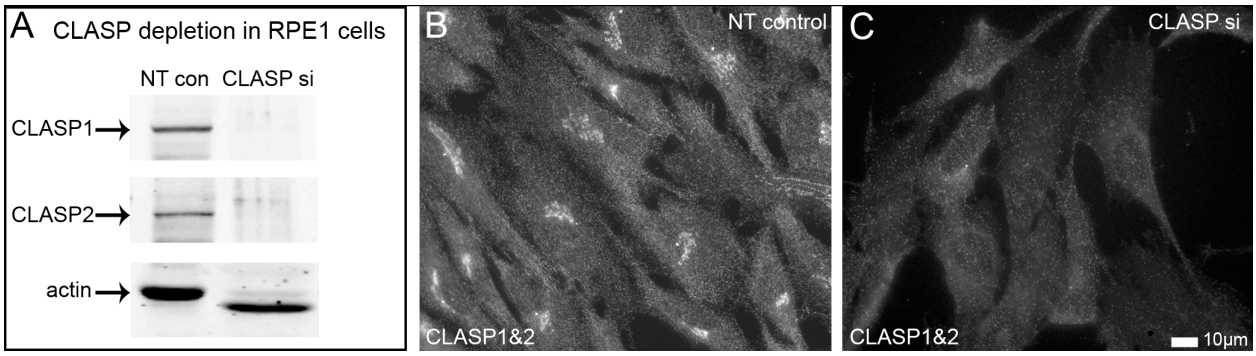

Figure S3: CLASP depletion in RPE1 cells. A, CLASP1 and CLASP2 detected by western blotting, actin, loading control. **B, C,** Immunostaining confirms that as compared with control non-targeted siRNA transfected cells (B), CLASPs are considerably depleted and evenly distributed in knockdown cell population (C)**.**

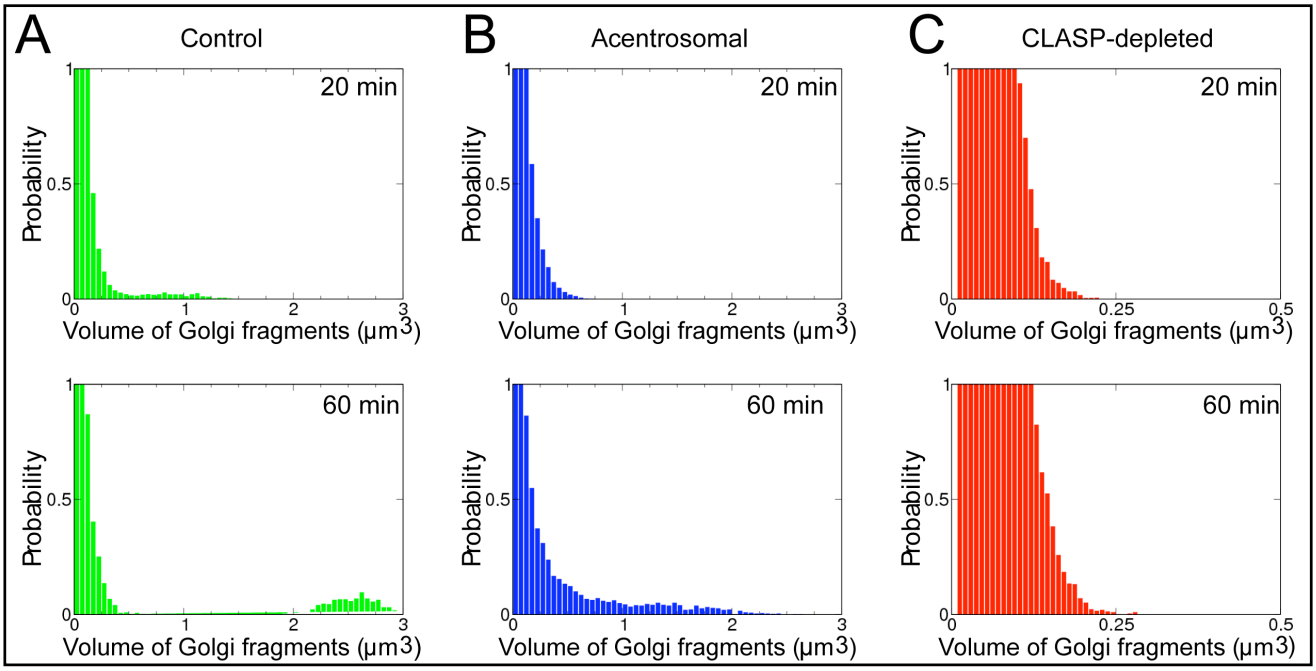

Figure S4: Predicted size distribution of Golgi fragments. Histograms of sizes are shown for 20 (top) and 60 (bottom) min of assembly. **A,** In control, the drift in size space starts after 20 min (see small number of ~ 1cubic micron-large fragments), and by 60 min a significant number of fragments are voluminous. Note that the total volume of large fragments is greater than that of small fragments. **B,** In the acentrosomal case, large fragments do appear, but their size distribution is very dispersed. **C,** In the CLASP-depleted case, large fragments do not evolve.

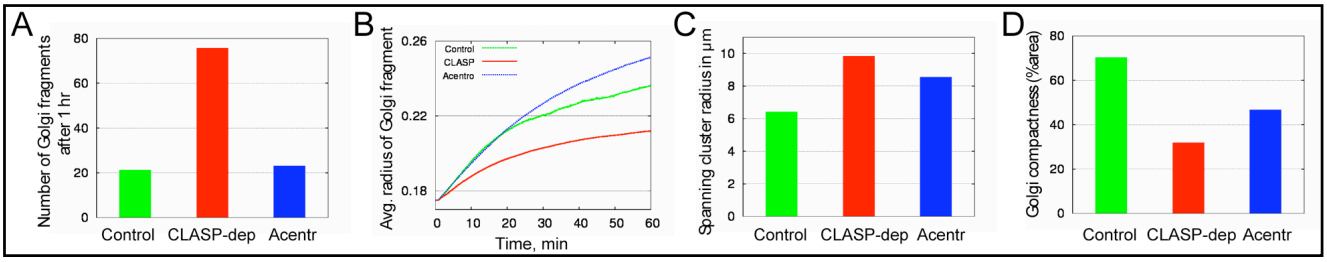

Figure S5: Predicted statistics of Golgi assembly. **A,** The total numbers of disjointed Golgi fragments is small and similar in control and acentrosomal cases, but is four-fold greater in the CLASP depleted case. **B**, Average radii of Golgi fragments in all 3 cases. **C,** Golgi fragments are distributed over a wider area in the CLASP depleted and acentrosomal cases after 60 min of assembly than in the control case. Spanning cluster's center is at the 'centre-of-mass' of all Golgi fragments, and its radius is R_{span} = sum (m_i r_i)/sum(r_i), where m_i and r_i are the volume and distance from the centre-of-mass of the i'th fragment. **D,** Predicted compactness of Golgi cluster for control, acentrosomal and CLASP depleted cases after 60 min of assembly. Compactness is defined as the ratio (Golgi area within spanning cluster)/(total area of the spanning cluster=πR_{span}^2).

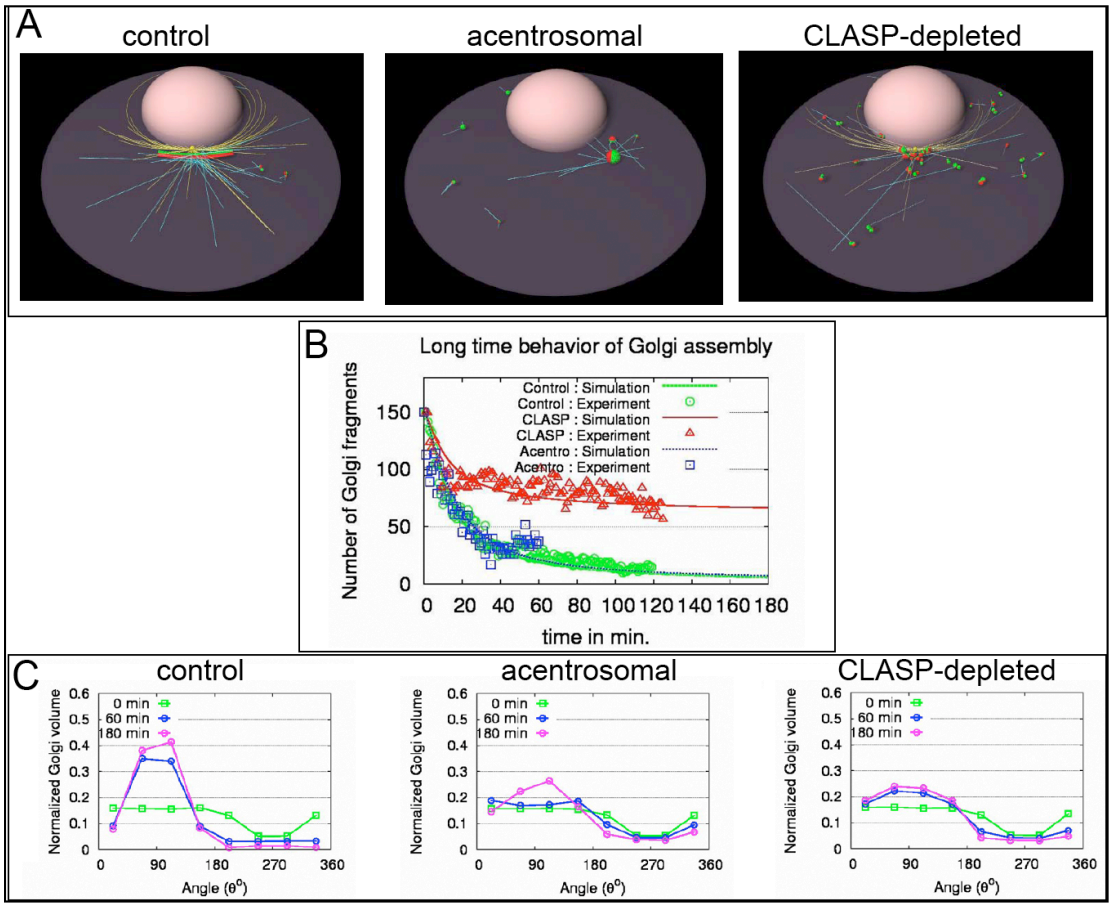

Figure S6: Predicted long term behavior of Golgi assembly. Overall Golgi organization (A), number of fragments (B) and angular distribution of the Golgi (C) do not differ significantly from those at 1 hour of assembly, indicating that the assembly has reached steady state at the 1 hour time point.

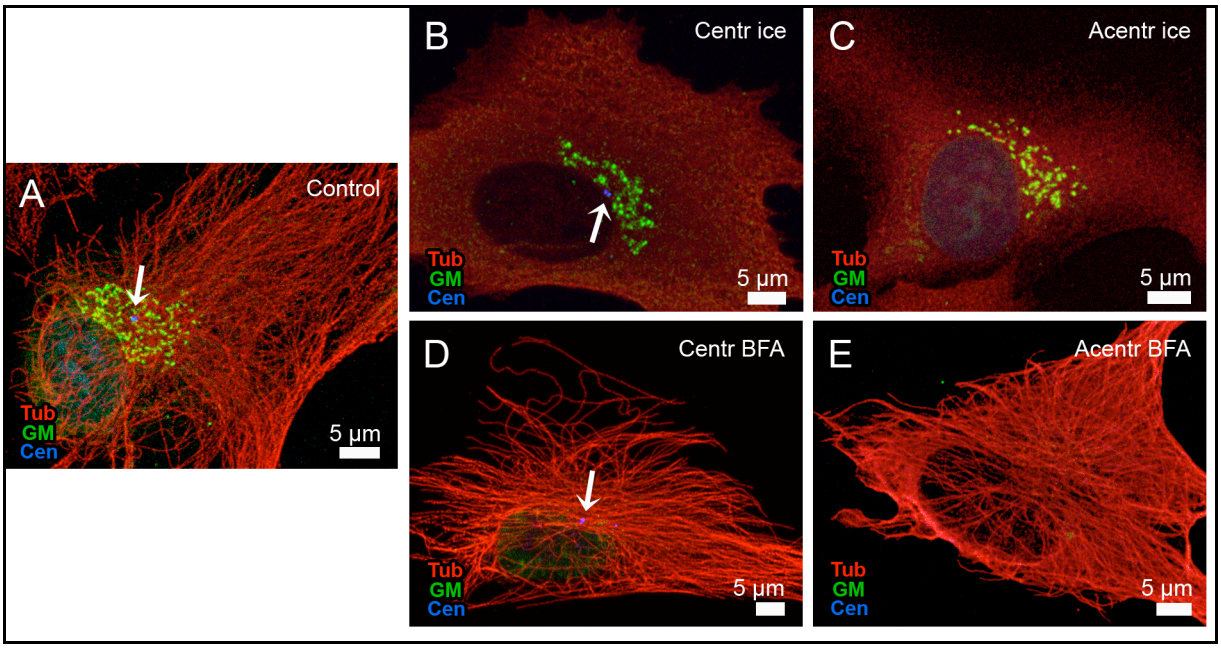

Figure S7: Independent disassembly of MTs and Golgi. Immunostaining. Tubulin, red, GM130, green (far red, false-colored). Centrin-GFP, blue (false-colored). In contrast to a control cell (A), cold-treated cells lack the MT network (B, C) and BFA-treated cells lack the Golgi apparatus (D, E). No striking difference observed between centrosomal (B, D) and acentrosomal cells (C, E).

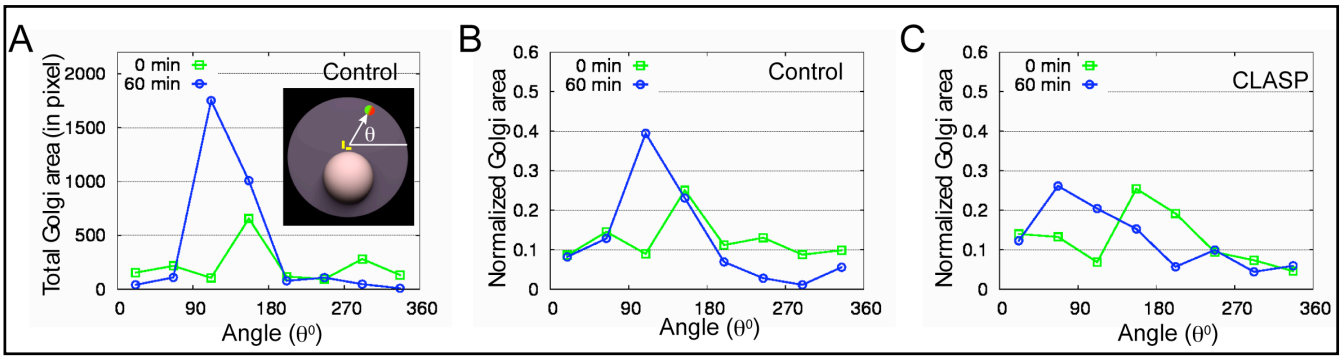

Figure S8: Experimental data for the angular distribution of Golgi fragments before (0 min) and after (60 min) assembly. **A,** Total area (in pixels) of Golgi fragments in each of the eight 45-degree wide sectors. The inset shows the geometry: zero degree corresponds to the right tangent to the nucleus from the centrosome. 90 degrees correspond to the outward normal to the nuclear surface. After 60 min of assembly, significant focusing in angular space takes place in control cell, and the most of Golgi ministacks are right in front of the centrosome. **B,** Normalized Golgi area averaged from 3 control cells shows the same effect as in A. **C,** In the CLASP depleted case (result from averaging 2-cell data), there is almost no focusing, and the maximum of the Golgi density deviates from 90 degrees.

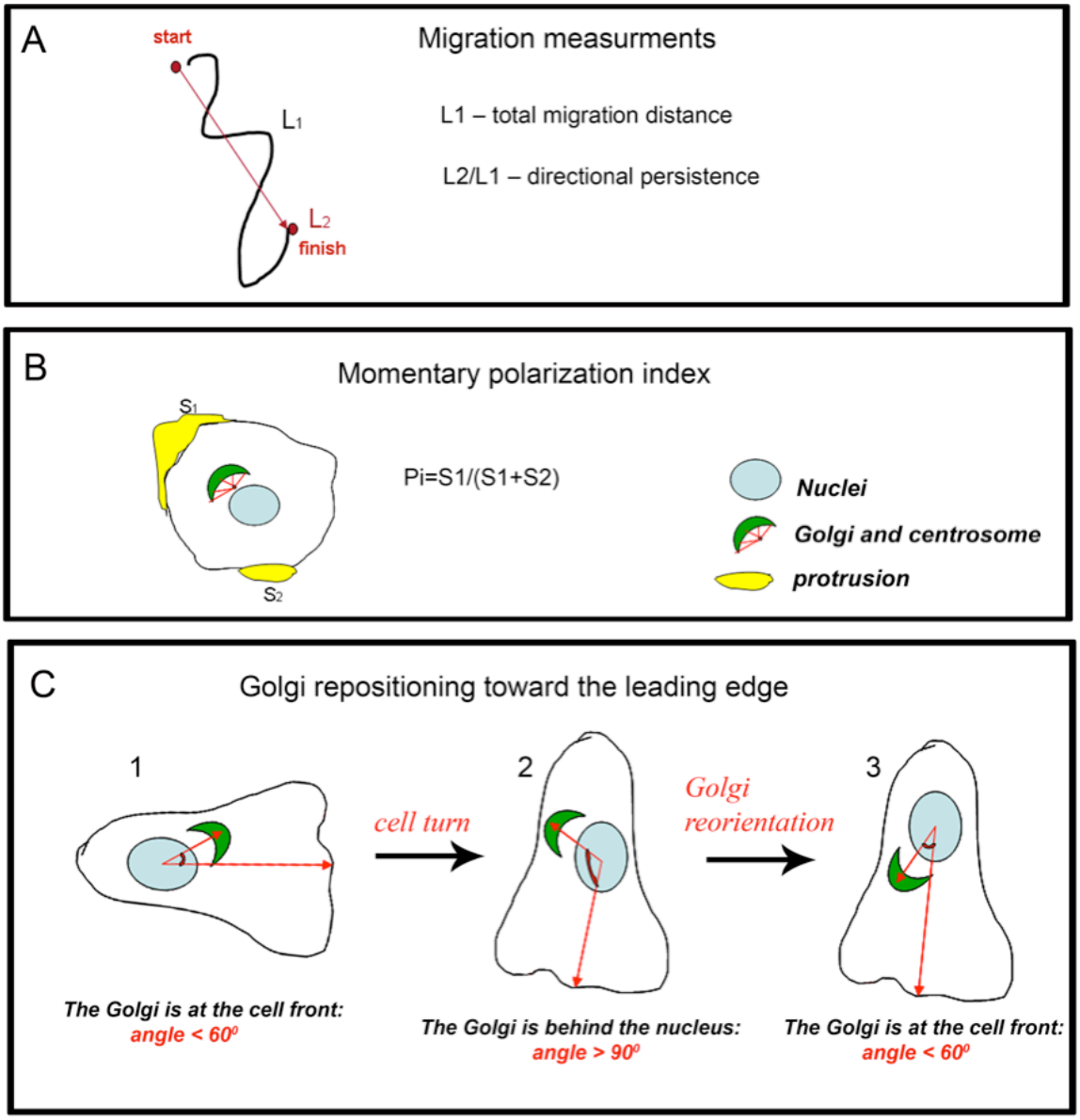

Figure S9. Metrics of the motility assays used in the study. A, Directional migration metric. Results of quantification are presented in Fig. 3 I, J. **B**, Momentary polarization metric. Results of quantification are presented in Fig. 3 K-O. **C**, Golgi repositioning metric. Time between cell configurations 2 and 3 is presented in Fig. 3P.

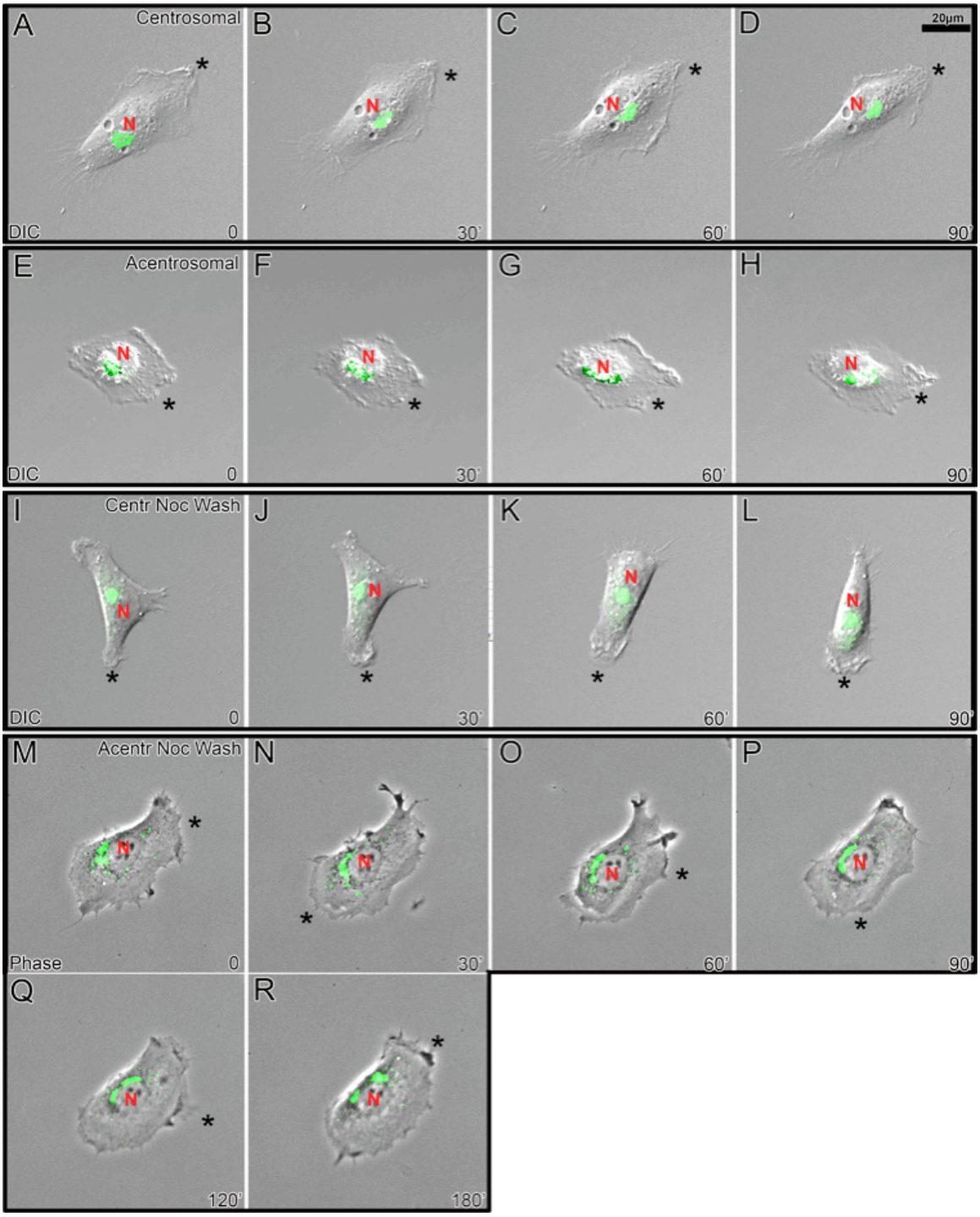

Fig S10. Repositioning of the Golgi during spontaneous turns in migrating cells. A-R, Selected frames from time-lapse movies presenting mCherry-Rab6 fluorescence (green) superimposed on DIC (A-L) or phase-contract (M-R) images. **A-D**, untreated centrosomal cell, **E-H**, untreated acentrosomal cell; **I-L,** centrosomal cell released from 2-hr nocodazole treatment; **M-R,** acentrosomal cell released from 2-hr after nocodazole washout. Time 0 corresponds to 2 hrs after nocodazole washout. Red letters *N* denote nuclei; asterisks denote leading edges.

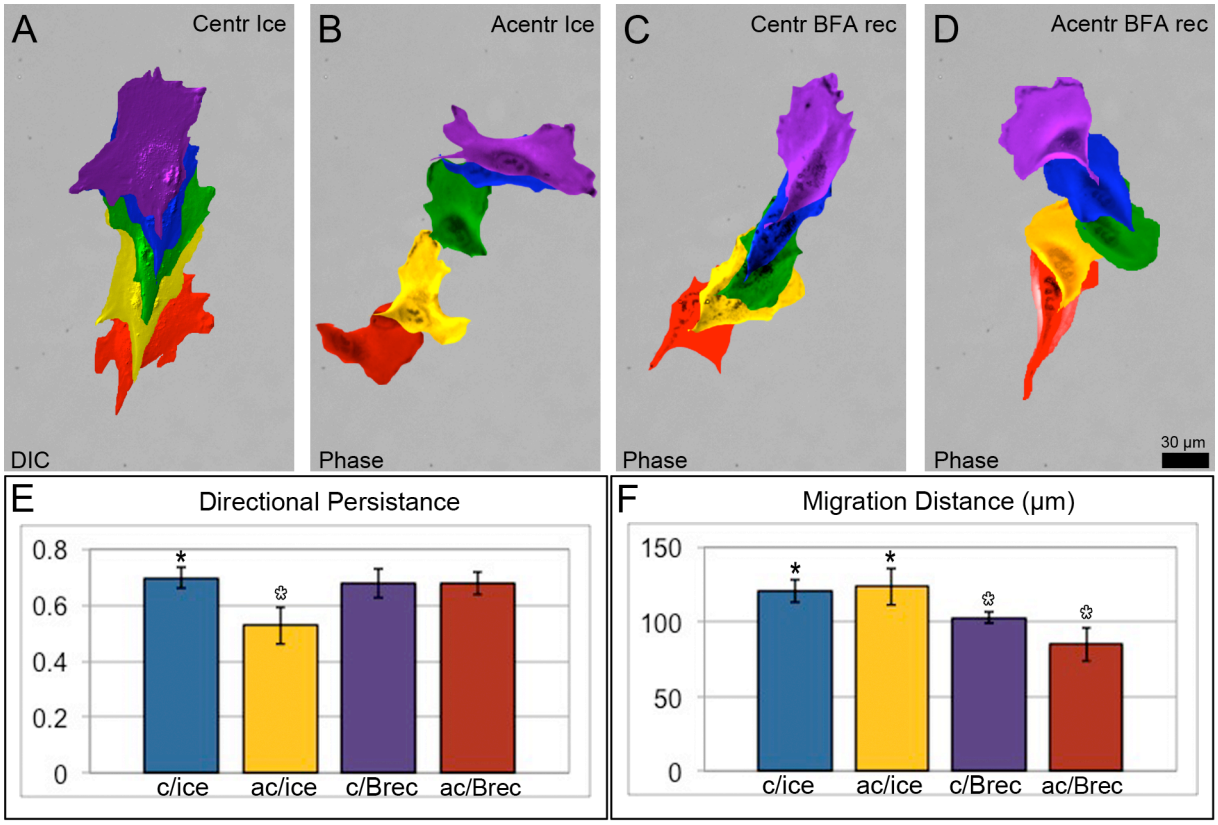

Fig. S11. Migration of centrosomal and acentrosomal cells after ice or BFA treatment. A-D, Random single cell migration of: **A**, centrosomal cell fixed 2h after ice treatment; **B**, acentrosomal cell starting 2h after ice treatment; **C**, centrosomal cell starting 2h after BFA washout; **D**, acentrosomal cell starting 2h after BFA washout. Color-coded images depict positions of each cell at 1h intervals. **E,** directional persistence of migration and **J,** total cell migration distance, in the four experimental conditions corresponding to A-D. Asterisk indicates $P<0.05$ in unpaired Student's t-test between bars marked with black and white asterisks. Error bars represent SEM.

Supplemental information on modeling Golgi assembly

To simulate Golgi assembly, we used agent-based object-oriented methodology (Alberts and Odell, 2004). Our discrete stochastic model is 3-dimensional. Parameters of the model are gathered in the table below. The geometry of the cell consists of an oblate-spheroidal space occluded by a spherical nucleus. Initially, ~ 150 Golgi fragments (ministacks) of radius 0.2 μm are uniformly randomly distributed within the cell space excluding the nuclear space. Experimental observations suggest that the cell and the nucleus are not concentric; the latter is usually located closer to the side of the cell. Therefore we assume certain displacement of the nuclear center relative to the cell center resembling observed geometry. The centrosome in the model, similar to the observation, is located near the nuclear surface, at the side distal to the cell boundary.

In the model, three classes of objects are implemented: (i) Golgi-generated and centrosomal MTs; (ii) Golgi fragments (ministacks, clusters); (iii) obstacles such as nuclear surface and cell boundary. The objects behave according to the rules described below. Golgi fragments are spherical; two hemispheres represent trans- and cis- sides respectively.

Simulated dynamic MTs are either linear or curved, as observed (with fixed radius of curvature close to that observed). Entire population of the centrosomal MTs is divided among the straight and curved MTs in a 2:1 ratio. This ratio is chosen because it appears to be optimal in terms of the speed and completeness of the assembly when varied between 1:1 and 3:1. A simple reason could be this: Because of excluded volume of the nucleus, straight centrosomal MTs can grow and span approximately 2/3 of the cell space. Therefore, remaining 1/3 space is given to the curved MTs to probe and catch targets. Each MT is represented by short rigid segments of equal lengths connected to each other. The minus-ends are anchored at the centrosome and Golgi, while the plus-ends undergo growth and shortening by adding or losing segments with constant rates V_g and V_s respectively. The catastrophe (f_{cat}) and rescue (f_{res}) frequencies are chosen to minimize the Golgi assembly time. Multiple simulations were made to find the optimal parameters. It turns out that the optimal regime corresponds to no rescues, f_{res} = 0 (MT growing in the direction where no Golgi fragments are located has to shrink to zero and start to grow in the new direction.) Optimal catastrophe frequency corresponds to MTs growing to the average length $<L_{MT}>$ comparable to the cell size; $f_{cat} = V_g / <L_{MT}>$. For simplicity we assumed these parameters to be the same for both centrosomal and Golgi-nucleated MTs.

A catastrophe also instantly takes place after a collision with the cell or nuclear boundary. Upon encountering a Golgi fragment, a MT may shrink or bypasses the Golgi fragment with probability P_{bypass} and grows further or catastrophes with probability (1 - P_{bypass}). We found that when probability P_{bypass} is below ~ 0.5, we could not fit the observed numbers of Golgi fragments as functions of time. For $0.5 < P_{bypass} < 1$, the fits were good. The reported results are for P_{bypass} = 0.8. About 300 dynamic MTs are nucleated from the centrosome in random directions spanning the whole space, as well as from the trans- sides of the Golgi stacks spanning the half space determined by orientation of each stack.

Once a growing MT plus-end encounters an initial Golgi fragment, we assume that dynein motor(s) associated with the membrane transport it toward the MT minus-end with speed V_{Golgi} determined by a free speed of the dynein motors. Viscous resistance of the cytoplasm is negligible (Cytrynbaum *et al.*, 2003). We assume that the motors coat the Golgi stacks on both cis- and trans- sides. We tested the case in which only trans- sides are associated with the motors, and the assembly was too slow to reproduce the data. Two fragments touching each other merge after certain delay time τ_{merge} but only if they were brought together by a Golgi-generated MT. Two fragments brought together accidentally by two centrosomal MTs merged only with a significant delay. The underlying mechanism is based on the idea that a MT-motor-

dependent action is required to allow the fragments to fuse with each other. Once two fragments are successfully merged, they form a single spherical fragment with the trans/cis surface pointing in the direction determined as the geometric average of the directions of the original two fragments. During this process, the entire MT array of participating fragments is destroyed and a new array of MTs emerges after the merging is completed. In the control case, the number of MTs nucleated by the fused fragment is assumed to be proportional to its surface area. (Number of MTs nucleated from the merged fragment = (Initial average number of MTs per Golgi fragment)*S_{merged}/S_{min}, where S_{merged} and S_{min} are the surface areas of the merged and initial fragments respectively.) Within the delay time $\tau_{merge,}$ if one of the engaged fragments is captured by MTs from a different source, it is pulled away and merging is not accomplished. When Golgi fragments are pulled by centrosomal MTs, they pile up near the centrosome. When a Golgi fragment was closer than a threshold to the centrosome and was above a certain radius, it flattened along the nuclear surface, due to pulling forces from the centrosomal MTs pressing the fragments to the nucleus.

We have considered three scenarios for the nucleation of MTs at the Golgi surface: A) control, B) acentrosomal, and C) CLASP depleted. The number of MTs nucleated by each initial Golgi fragment is 3 - 4 in cases (A,B), 1 - 2 in case (C). In case (B), the centrosomal MT array is completely disrupted.

The polarization parameter reported in Fig. 4E was computed as the integral

$$\frac{\int_0^{2\pi} \cos(\theta - \theta_0) \times f(\theta) d\theta}{\int_0^{2\pi} f(\theta) d\theta}$$, where $f(\theta)$ is the angular distribution of the MTs, and θ_0 is the direction from the center of the nucleus to the centrosome.

We have simulated the model repeatedly varying parameters and repeating assembly simulations hundreds of times for each parameter value. Technical details of the simulations are the same as those reported in (Paul *et al.*, 2009). The numerical codes were implemented with C programming language. Numerical experiments were performed on an IBM dual CPU Opteron server.

Parameters used in the simulation

Parameter	Description	Value
R_{cell}	Cell radius	20-30 μm *
d_{cell}	Cell thickness	1-1.5 μm *
R_{nuc}	Nuclear radius	10 μm *
R_{ves}	Initial Golgi fragment radius	0.15-0.2 μm *
NMT_{cent}	Number of centrosomal MTs	250-300 **
NMT_{Golgi}	Number of initial MTs per Golgi fragment	0-5 ***
V_{Golgi}	Dynein-driven speed of a small fragment	0.13 μm s^{-1} ****
V_g	MT growth rate	0.1 μm s^{-1} **
V_s	MT shortening rate	0.2 μm s^{-1} **
f_{cat}	Optimal MT catastrophe frequency	0-0.002 s^{-1} *****
f_{res}	Optimal MT rescue frequency	0 s^{-1} *****
Z_{shift}	Shift of the nuclear center from the cell center	-10 μm *
H_{cent}	Centrosome distance from nucleus	1.35 μm *
τ_{merge}	Ministack merging time	1 min ******
τ_{flip}	Ministack flip time	1.5 min ******
σ_{MT}	Number of MTs nucleated per μm^2 surface area of a merged Golgi fragment	~ 4 ***
P_{bypass}	Probability for a MT plus-end that runs into a Golgi fragment to bypass it	~ 0.5 – 1 ***

* Based on our observations (this study): four cell images were used. For the radii, we measured the areas of the cell, nucleus and Golgi fragments, divided it by π, took the square root, and averaged for four images. We averaged the cell thickness from the side view along the length of the cell, and then averaged for four images.

** (Rusan *et al.*, 2001; Burakov *et al.*, 2003; Paul *et al.*, 2009).

*** Inferred from from fitting the number of Golgi fragments as function of time, as well as based on previous results (Efimov *et al.*, 2007).

**** (Cytrynbaum *et al.*, 2003).

***** Obtained by numerical scan of the parameter space. Specifically, starting with 150 Golgi fragments, we ran the simulation for the control case and measured the time until the fragment number reduced to 25. The simulations were performed in the range of the catastrophe and rescue frequencies between 0 and 0.05/s with increment 0.001/s. We then plotted the assembly time as a function of catastrophe and rescue frequencies and determined their optimal values from the global minima of the obtained assembly time. The optimal frequency of rescue turned out to be lower than that reported for the peripheral parts of interphase cells. Our simulations predict that the Golgi assembly would slow down considerably if the rescue frequency is as high as reported for the peripheral parts of interphase cells. Interestingly, the frequency of rescue needed to best fit the experimental data resembles the frequency observed during prometaphase (Paul *et al.*, 2009). Note that interphase MT parameters were measured in steady-state while during prometaphase a new array of microtubules is assembled. The latter condition is more similar to the situation observed upon nocodazole washout.

****** These are maximal times that give good numerical fits to the data. Smaller times do not make the fits worse; greater times worsen the fits.

Supplemental Experimental Procedures and Data Analysis

The Golgi complex organization

Circularity and Compactness

For these measurements the Golgi was visualized via immunostaining for the cis-Golgi component GM130. The complex was freehand-outlined in maximal-intensity projections computed from complete Z-series collected at 0.2 μm steps.

ImageJ circularity plugin (rsb.info.nih.gov/ij/plugins/circularity.html) was used to compute the Circularity index [$Circularity = 4\pi*(area/perimeter^2)$].

Circularity index has been used to analyze overall cell shape (Patel *et al.*, 2008; Miller *et al.*, 2009) as well as to measure microfilament ring circularity during cellularization (Thomas and Wieschaus, 2004). A circularity value of 1 corresponds to a perfect circle.

To determine compactness the freehand-outline of the Golgi was thresholded to assign an integer pixel value within the selection and 0 value to the background. An imageJ plugin that calculates the percentage of non-zero pixels in the image or selection was used to determine the percentage of the area taken by the Golgi stacks inside the selection. Higher level of compactness indicates more dense Golgi structure while lower level of compactness corresponds to more dispersed and disorganized Golgi complex.

Post-Golgi vesicles tracking

Two-minute time-lapse wide-field fluorescence sequences of RPE1 cells expressing fluorescently-labeled Rab6 were recorded at 1-s intervals. Individual particles were tracked manually using the MTrackJ ImageJ plugin (www.imagescience.org/meijering/software/mtrackj/) Then the number of tracks was determined in each quadrant oriented with respect to the position of the cell's leading edge (front, left, back and right quadrants).

Directional persistence of cell migration.

4-hr long time-lapse DIC sequences were recorded at 3-min intervals. Positions of the nucleus were tracked manually using the MTrackJ ImageJ plugin (see above). Cell relocation was measured as the distance between the nucleus position at the start and at the finish. The length of tracks was deemed to represent the total distance of cells migration. Directional persistence was calculated as cell relocation divided by the length of the track (Fig. S2A). Directional persistence value of 1 corresponds to the strictly uni-directional migration.

Momentary polarity index

To evaluate ability of a cell to persistently maintain polarity, 30-min long time-lapse DIC sequences were recorded at 3-min intervals. Cell contours were freehand-outlined at each time-point. These outlines were superimposed on the next frame in the sequence, which allowed us to identify new-formed protrusions (Fig. S2B). Momentary polarity index was calculated as the ratio of the area of protrusion at the leading edge to the summarized area of protrusions along the whole cell perimeter. Momentary polarity index value of 1 indicates a maximally polarized cell, and value of ½ corresponds to an absolutely non-polarized cell.

The Golgi reorientation assay

To measure the time required for Golgi reorientation to the leading edge, multi-mode DIC/fluorescence time-lapses were recorded at 3-min intervals. Positions of the cell nucleus, the Golgi complex and the leading edge were manually tracked using MTrackJ ImageJ plugin (see above). For each frame, the angle between position of the Golgi complex center and the leading edge center with angular point corresponding to nucleus position was measured (Fig. S2C). An acute angle below 60^0 corresponded to the front position of the Golgi according to the leading edge, and an obtuse angle (over 90^0) corresponded to the back position. Time from the cell turn (new leading edge formation) and the Golgi re-orientation toward the leading edge (below 60^0) was measured for sharp turns upon which the Golgi was found behind the nucleus (at least 90^0 angle).

Supplemental References

Alberts, J.B., and Odell, G.M. (2004). In silico reconstitution of Listeria propulsion exhibits nano-saltation. PLoS Biol *2*, e412.

Burakov, A., Nadezhdina, E., Slepchenko, B., and Rodionov, V. (2003). Centrosome positioning in interphase cells. J Cell Biol *162*, 963-969.

Cytrynbaum, E.N., Scholey, J.M., and Mogilner, A. (2003). A force balance model of early spindle pole separation in Drosophila embryos. Biophys J *84*, 757-769.

Efimov, A., Kharitonov, A., Efimova, N., Loncarek, J., Miller, P.M., Andreyeva, N., Gleeson, P., Galjart, N., Maia, A.R., McLeod, I.X., Yates, J.R., 3rd, Maiato, H., Khodjakov, A., Akhmanova, A., and Kaverina, I. (2007). Asymmetric CLASP-dependent nucleation of noncentrosomal microtubules at the trans-Golgi network. Dev Cell *12*, 917-930.

Miller, P.M., Folkmann, A.W., Maia, A.R., Efimova, N., Efimov, A., and Kaverina, I. (2009). Golgi-derived CLASP-dependent microtubules control Golgi organization and polarized trafficking in motile cells. Nat Cell Biol *11*, 1069-1080.

Patel, H., Konig, I., Tsujioka, M., Frame, M.C., Anderson, K.I., and Brunton, V.G. (2008). The multi-FERM-domain-containing protein FrmA is required for turnover of paxillin-adhesion sites during cell migration of Dictyostelium. J Cell Sci *121*, 1159-1164.

Paul, R., Wollman, R., Silkworth, W.T., Nardi, I.K., Cimini, D., and Mogilner, A. (2009). Computer simulations predict that chromosome movements and rotations accelerate mitotic spindle assembly without compromising accuracy. Proc Natl Acad Sci U S A *106*, 15708-15713.

Rusan, N.M., Fagerstrom, C.J., Yvon, A.M., and Wadsworth, P. (2001). Cell cycle-dependent changes in microtubule dynamics in living cells expressing green fluorescent protein-alpha tubulin. Mol Biol Cell *12*, 971-980.

Thomas, J.H., and Wieschaus, E. (2004). src64 and tec29 are required for microfilament contraction during Drosophila cellularization. Development *131*, 863-871.